

Effects of Heteroatom Substitution on the Structures, Physicochemical Properties, and Redox Behavior of Nickel(II) Complexes with Pyridine-Containing Macrocyclic Ligands

Masayasu Taki,*[1,2] Yoshiaki Kawashima,[1] Naoko Sakai,[1] Tasuku Hirayama,[1] and Yukio Yamamoto[1]

[1]Graduate School of Human and Environmental Studies, Kyoto University, Yoshida, Sakyo-ku, Kyoto 606-8501

[2]Graduate School of Global Environmental Studies, Kyoto University, Yoshida, Sakyo-ku, Kyoto 606-8501

Received October 11, 2007; E-mail: taki@chem.mbox.media.kyoto-u.ac.jp

Nickel(II) complexes supported by 14-membered pyridine-containing macrocyclic ligands $\mathbf{L^E}$ (E = NH, S, and O), represented as $[Ni^{II}(\mathbf{L^{NH}})](ClO_4)_2$ (**1a**), $[Ni^{II}(\mathbf{L^S})](ClO_4)_2$ (**2a**), $[Ni^{II}(\mathbf{L^S})](ClO_4)(BPh_4)$ (**2b**), $[Ni^{II}(\mathbf{L^O})(CH_3CN)_2](ClO_4)_2$ (**3a**), and $[Ni^{II}(\mathbf{L^O})(CH_3CN)_2](ClO_4)(BPh_4)$ (**3b**), have been synthesized. X-ray crystal structures of complexes **1a** and **2b** have square-planar structures in low-spin state, whereas complex **3b** exhibits an octahedral high-spin configuration where two solvent molecules occupy the axial positions of the NiN_3O_1 plane. The absorption spectra of **1a** and **2a** in coordinating solvents show interconversion of high-/low-spin states, for which the equilibrium constants and thermodynamic parameters (ΔH^0 and ΔS^0) have been determined. However, in the case of complex **3a** in coordinating solvent, the high-spin state dominates at temperatures ranging from −40 to 60 °C. Cyclic voltammetry of the complexes **1a** and **2a** in CH_3CN showed a reversible wave for a Ni^{II}/Ni^{I} redox couple. The redox potential for **2a** ($E_{1/2} = -1.20$ V vs. $Ag/AgNO_3$) is more positive than that for **1a** ($E_{1/2} = -1.48$ V). In contrast to these complexes, **3a** showed an irreversible redox couple with a significantly large peak separation of 460 mV. This result indicates that the coordination geometries of the nickel complex **3a** drastically change between six-coordinate Ni^{II} and four-coordinate Ni^{I} states.

Tuning spin states of nickel(II) complexes, square-planar low-spin ($^1A_{1g}$) and octahedral high-spin ($^3B_{1g}$), has been one of the most attractive research objectives not only in the fields of inorganic and biological chemistry[1–3] but also in the perspective of creating molecular switches.[4] The equilibrium of spin-state interconversion in Ni^{II} complexes depends on many factors such as temperature, counter anions, solvents, and ionic strength of aqueous solution,[5–9] and has been utilized to develop fluorescent molecular switches, where fluorescence "on" and "off" are controlled by low- and high-spin states of Ni^{II} ion, respectively.[4] The interconversion of the spin state is also found in F_{430} cofactor in methyl-coenzyme M reductase (MCR),[10] which catalyzes methane formation from methyl-coenzyme M and coenzyme B. Six-coordinate bis-aqua $S = 1$ species is favored at low temperature, while at high temperature the four-coordinate $S = 0$ form dominates.[11,12] Furthermore, in this enzymatic system, the nickel ion in F_{430} is redox active and is found to be in an EPR-active Ni^{I} form in which the nickel center is square planer $S = 1/2$ with a $(3d_{x^2-y^2})^1$ electronic ground state.[13,14]

Among numerous Ni^{II} complexes so far reported, those having cyclam (1,4,8,11-tetraazacyclotetradecane) and its analogs as macrocyclic ligands have been particularly investigated to explore the alkyl and heteroatom substituent effects of the ligand framework on the spin-state interconversion and the electrochemical properties.[15–18] However, detailed investigations of the structural and physicochemical properties of Ni^{II} complexes supported by pyridine-containing macrocycles have been rarely reported[19–24] although the coordination chemistry of these ligands has attracted much attention due to the effective coordination ability of pyridine.[25]

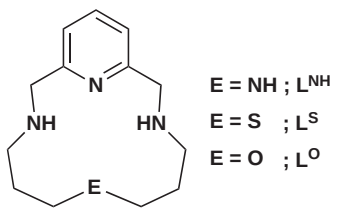

Scheme 1.

In this study, we have employed a pyridine-containing 14-membered macrocyclic ligand, 3,7,11,17-tetraazabicyclo-[11.3.1]heptadeca-1(16),13(17),14-triene[22] ($\mathbf{L^{NH}}$), and its thia- and oxa-derivatives[26] ($\mathbf{L^S}$ and $\mathbf{L^O}$, respectively), where the nitrogen atom at the 7-position of $\mathbf{L^{NH}}$ is replaced with a sulfur or an oxygen atom (Scheme 1). As for the nickel(II) complexes supported by the mixed-donor macrocycles containing hard, soft, and borderline donors, the crystal structures, electronic spectroscopies, and redox behaviors have been investigated in order to shed light on the effects of the coordinative heteroatom on the complexes.

Results and Discussion

Synthesis and Structural Characterization. All macrocyclic ligands $\mathbf{L^E}$ (E = NH, S, and O) were synthesized by demetallation reaction of the corresponding Cu^{II} complexes prepared by known copper-template condensation reaction of 2,6-pyridinedicarbaldehyde and appropriate diamines followed by reduction of diimines with $NaBH_4$. The low yields for $\mathbf{L^O}$ and $\mathbf{L^S}$ are due to the formation of by-products, linear amino–

Published on the web May 14, 2008; doi:10.1246/bcsj.81.590

alcohols, arisen from incomplete formation of the macrocycles and the following reduction of the aldehyde groups. The yields of the desired macrocyclic ligands did not increase even when the condensation reactions were continued for another couple of hours.

Treatment of $Ni(ClO_4)_2 \cdot 6H_2O$ with an equimolar amount of the ligands in methanol gave the corresponding Ni^{II} complexes as the perchlorate salts, **1a**–**3a**, all of which were recrystallized by vapor diffusion of diethyl ether into an CH_3CN solution of each Ni^{II} complex prior to measurements. In the case of $\mathbf{L^{NH}}$ and $\mathbf{L^{S}}$, Ni^{II} complexes were obtained as orange crystals, whereas the Ni^{II} complex of $\mathbf{L^{O}}$ was given as pale-purple crystals. X-ray crystal structure determination of **2a** and **3a**, unfortunately, gave structures with very high R values (>0.25) although R merge values observed after data collection were low enough at ≈ 0.04. Several attempts to decrease the R values of **2a** and **3a** were not successful, therefore, the perchlorate anions of these complexes were exchanged with BPh_4^- in methanol as described in the experimental section. The resulting complexes, **2b** and **3b**, were recrystallized again to afford single crystals suitable for X-ray diffraction. The ORTEP drawings of Ni^{II} complexes **1a**, **2b**, and **3b** are shown in Figure 1, the summaries of the crystal data and the experimental parameters are given in Table 1, and the selected bond lengths and angles are listed in Table 2. It should be noted that all of these Ni^{II} complexes, which contain perchlorate anions, are explosive. In fact, we have encountered explosion of the complexes in all attempts of elemental analysis, which results in large experimental errors exceeding 5% in nitrogen. Thus, we strongly suggest that the materials should be handled carefully in small amounts.

Ni^{II} complex with $\mathbf{L^{NH}}$, $[Ni^{II}(\mathbf{L^{NH}})](ClO_4)_2$ (**1a**), exhibits a square-planar geometry coordinated by a pyridine nitrogen atom and three secondary amines, with a distance of $\rho = 0.105$ Å between the least-square N_4 plane and the metal ion center. The distortion from square-planar geometry of 0.105 Å is almost identical to that in the square-planar Cu^{II} complex of $\mathbf{L^{HN}}$ ($\rho = 0.133$ Å).[18] No additional ligand such as solvents was coordinated even though **1a** was recrystallized from an CH_3CN solution. The perchlorate anions in the crystal lattice lie above and below the plane of the Ni^{II} complex, however, the distances between the nearest oxygen atom of each perchlorate ion and the metal ion center are 3.055 and 3.139 Å, indicating no significant influence on the Ni^{II} center. The bond lengths of Ni–N (1.842–1.944 Å) in **1a** are typical for low-spin Ni^{II} complexes formed by nitrogen donor atoms. These finding are in contrast to the crystal structure of the high-spin Ni^{II} complex of cyclam $[Ni^{II}(cyclam)(CH_3CN)_2](ClO_4)_2$ reported by Fabbrizzi and his co-workers, in which two solvent molecules occupy the axial positions when recrystallized from an CH_3CN solution.[8] The structural difference between the two ligand systems, cyclam and $\mathbf{L^{NH}}$, may be attributed to the difference both in the electron-donor basicity of amine and pyridine nitrogen atoms (i.e. sp^3 and sp^2 donors) and in the chelate ring sequences (5,6,5,6 and 5,5,6,6 macrocycles for cyclam and $\mathbf{L^{NH}}$, respectively).

The overall structure of the Ni^{II} complex with $\mathbf{L^{S}}$, $[Ni^{II}(\mathbf{L^{S}})](ClO_4)(BPh_4)$ (**2b**), is essentially the same as that of **1a**, where the metal ion center displays a square-planar geometry and Ni^{II} is low-spin state. In this case, one of the two perchlorate anions was replaced by BPh_4^- by anion exchange with $NaBPh_4$. The equatorial plane of **2b** has the N_3S_1 donor set, where the bond lengths of Ni–N are in the range of 1.842–1.950 Å and Ni–S bond length is 2.166 Å, in close agreement with reported low-spin Ni^{II} complexes having an N_2S_2 or N_3S_1 coordination environment.[27,28] Interestingly, a 3,11-dithia derivative of $\mathbf{L^{NH}}$, 3,11-dithia-7,17-diazabicyclo-[11.3.1]heptadeca-1(17),13,15-triene, reported by Lodeiro et al. forms high-spin state Ni^{II} complexes in the solid state,[20] while the sulfur substitution at 7-position, that is $\mathbf{L^{S}}$, affords low-spin of Ni^{II}. To the best of our knowledge, **2b** is the first

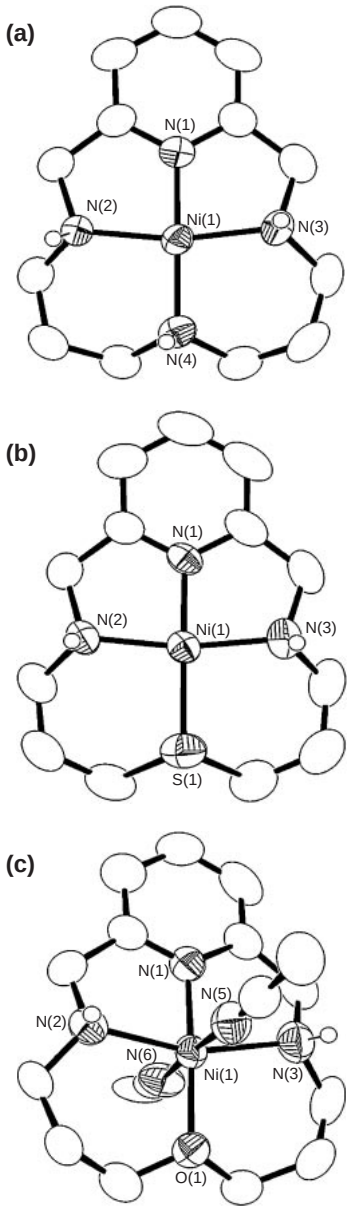

Figure 1. ORTEP drawings of the cationic parts of (a) $[Ni^{II}(\mathbf{L^{NH}})](ClO_4)_2$ (**1a**), (b) $[Ni^{II}(\mathbf{L^{S}})](ClO_4)(BPh_4)$ (**2b**), and (c) $[Ni^{II}(\mathbf{L^{O}})(CH_3CN)_2](ClO_4)(BPh_4)$ (**3b**) showing 50% thermal ellipsoids. The counter anions and the hydrogen atoms except on nitrogen atoms are omitted for clarity.

Table 1. Summary of X-ray Crystallographic Data for **1a**, **2b**, and **3b**

	1a	**2b**	**3b**
Empirical formula	$C_{13}H_{22}N_4NiO_8Cl_2$	$C_{37}H_{41}N_3BSNiClO_4$	$C_{41}H_{47}N_5BO_5NiCl$
Formula weight	491.94	728.77	794.82
Crystal system	orthorhombic	orthorhombic	triclinic
Space group	*Pbca* (#61)	*Pbca* (#61)	$P\bar{1}$ (#2)
a/Å	9.0616(9)	16.3226(3)	10.1811 (9)
b/Å	13.6971(17)	16.1306(3)	12.9018 (9)
c/Å	31.022(3)	25.6670(5)	17.1777(13)
α/deg	90	90	79.812(2)
β/deg	90	90	85.488(3)
γ/deg	90	90	66.555(2)
V/Å^3	3850.3(7)	6758.0(2)	2037.4(3)
Z	8	8	2
$F(000)$	1524.00	3056.00	836.00
D_{calcd}/g cm^{-3}	1.697	1.432	1.296
T/°C	−100	−70	23
Crystal size/mm^3	0.50 × 0.30 × 0.10	0.40 × 0.30 × 0.30	0.50 × 0.50 × 0.20
μ(Mo Kα)/cm^{-1}	13.352	7.607	5.905
Diffractometer	Rigaku RAXIS-RAPID	Rigaku RAXIS-RAPID	Rigaku RAXIS-RAPID
Radiation	Mo Kα (0.71075 Å)	Mo Kα (0.71075 Å)	Mo Kα (0.71075 Å)
$2\theta_{max}$/deg	54.9	55.0	55.0
No. of reflns measd	34132	69830	20080
No. of observations	13230 [$I > 2.00\sigma(I)$]	33433 [$I > 2.00\sigma(I)$]	9302 [$I > 2.00\sigma(I)$]
No. of variables	275	474	534
R[a)]	0.062	0.055	0.086
wR_2[b)]	0.136	0.123	0.239
GOF[c)]	0.997	1.008	1.003

a) $R = \Sigma(|F_o| - |F_c|)/\Sigma|F_o|$. b) $wR_2 = \{\Sigma(w(F_o^2 - F_c^2)^2/\Sigma wF_o\}^2\}^{1/2}$. c) Goodness of fit on F^2.

Table 2. Selected Bond Lengths (Å) and Angles (°)

	$[Ni^{II}(\mathbf{L^{NH}})](ClO_4)_2$ (**1a**)		
Ni(1)–N(1)	1.842(2)	Ni(1)–N(2)	1.936(2)
Ni(1)–N(3)	1.944(2)	Ni(1)–N(4)	1.937(2)
N(1)–Ni(1)–N(2)	84.37(9)	N(1)–Ni(1)–N(3)	83.24(9)
N(1)–Ni(1)–N(4)	179.52(9)	N(2)–Ni(1)–N(3)	162.20(11)
N(2)–Ni(1)–N(4)	95.33(9)	N(3)–Ni(3)–N(4)	96.98(9)
	$[Ni^{II}(\mathbf{L^{S}})](ClO_4)_2$ (**2b**)		
Ni(1)–N(1)	1.8413(13)	Ni(1)–N(2)	1.9467(13)
Ni(1)–N(3)	1.9500(13)	Ni(1)–S(1)	2.1663(5)
N(1)–Ni(1)–N(2)	84.39(5)	N(1)–Ni(1)–N(3)	84.73(5)
N(1)–Ni(1)–S(1)	170.84(3)	N(2)–Ni(1)–N(3)	166.47(5)
N(2)–Ni(1)–S(1)	94.45(4)	N(3)–Ni(1)–S(1)	95.02(4)
	$[Ni^{II}(\mathbf{L^{O}})(CH_3CN)_2](BPh_4)(ClO_4)$ (**3b**)		
Ni(1)–N(1)	1.956(4)	Ni(1)–N(2)	2.064(4)
Ni(1)–N(3)	2.065(4)	Ni(1)–N(4)	2.131(5)
Ni(1)–N(5)	2.107(6)	Ni(1)–O(1)	2.039(3)
N(1)–Ni(1)–N(2)	80.97(17)	N(1)–Ni(1)–N(3)	82.12(18)
N(1)–Ni(1)–N(4)	94.20(19)	N(1)–Ni(1)–N(5)	87.4(2)
N(1)–Ni(1)–O(1)	174.81(19)	N(2)–Ni(1)–N(3)	160.6(2)
N(2)–Ni(1)–N(4)	86.42(19)	N(2)–Ni(1)–N(5)	96.4(2)
N(2)–Ni(1)–O(1)	98.58(16)	N(3)–Ni(1)–N(4)	85.3(2)
N(3)–Ni(1)–N(5)	92.3(2)	N(3)–Ni(1)–O(1)	99.12(17)
N(4)–Ni(1)–N(5)	176.97(16)	N(4)–N(1)–O(1)	90.93(17)
N(5)–Ni(1)–O(1)	87.54(18)		

structurally characterized low-spin Ni^{II} complex supported by a macrocyclic ligand containing a pyridine ring and a thioether in the coordination sphere.

In contrast to the cases of $\mathbf{L^{NH}}$ (**1a**) and $\mathbf{L^{S}}$ (**2b**), a Ni^{II} complex of $\mathbf{L^{O}}$, $[Ni^{II}(\mathbf{L^{O}})(CH_3CN)_2](ClO_4)(BPh_4)$ (**3b**), adopts a six-coordinate geometry in which two CH_3CN molecules provided by the recrystallization solvent occupy the axial positions of NiN_3O_1 plane. The average bond length between Ni^{II} and the three nitrogen atoms of the ligand $\mathbf{L^{O}}$ is 2.028 Å and the axial Ni–N bond lengths are 2.131 and 2.107 Å. Judging from the structural geometry and its bond lengths in the coordination sphere, **3b** is expected to be in the high-spin state of Ni^{II}. The crystal structure of **3a** is essentially the same as that of **3b**, where two CH_3CN molecules coordinate to the Ni^{II} center forming an octahedral geometry, although the crystallographic data were less satisfactory for publication as mentioned above. In fact, the spin state of $[Ni^{II}(\mathbf{L^{O}})(CH_3CN)_2](ClO_4)_2$ (**3a**) was confirmed to be high-spin ($S = 1$) by magnetic susceptibility measurement, where the effective magnetic moment is 3.17 μ_B at room temperature. Thus, replacement of only one nitrogen atom at the 7-position of macrocyclic ligand $\mathbf{L^{NH}}$ with an oxygen atom drastically alters the spin state of the Ni^{II} complex in solid state, whereas the thioether analog of $\mathbf{L^{NH}}$ gives no significant change in the coordination geometry of the metal center. Because steric crowding around the metal ion in these three Ni^{II} complexes can be considered to be similar, these structural differences may be related to the electron donation tendencies of N, S, and O atoms in the 14-membered macrocyclic ligand. An oxygen atom, which is a

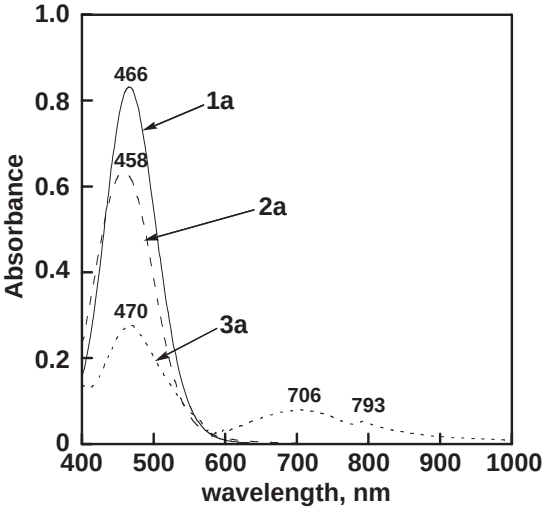

Figure 2. Absorption spectra of $[Ni^{II}(\mathbf{L^{NH}})](ClO_4)_2$ (**1a**, solid line), $[Ni^{II}(\mathbf{L^{S}})](ClO_4)_2$ (**2a**, dashed line), and $[Ni^{II}(\mathbf{L^{O}})(CH_3CN)_2](ClO_4)_2$ (**3a**, dotted line) in CH_3NO_2 at 20 °C. [Ni^{II} complex] = 5.0×10^{-3} M.

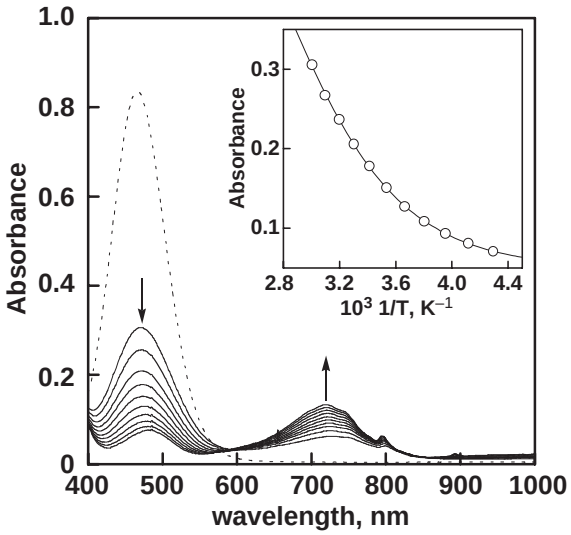

Figure 3. Absorption spectral change observed upon decreasing the temperature from 60 to −40 °C in CH_3CN solution of $[Ni^{II}(\mathbf{L^{NH}})](ClO_4)_2$ (**1a**, 5.0×10^{-3} M). Dotted line represents the absorption spectrum of **1a** measured in CH_3NO_2 at 20 °C. Inset: Plots of the absorbance at 468 nm against $1/T$ with best fit curve for A_H, ΔH^0, and ΔS^0 of 0.05, −18.4 kJ mol^{-1}, and −48.9 J K^{-1} mol^{-1}, respectively.

weaker donor than nitrogen and sulfur atoms, may increase Lewis acidity of the Ni^{II} center, enhancing the axial bonding interaction.

Absorption Spectra of Ni^{II} Complexes in Non-Coordinating Solvent. The absorption spectra of complexes **1a**–**3a** were measured in a non-coordinating solvent such as CH_3NO_2 (Figure 2), the spectral data (λ_{max} and ε) of all complexes are summarized in Table 3. Complexes **1a** and **2a** exhibit an intense absorption band at 466 nm ($\varepsilon = 167\,M^{-1}\,cm^{-1}$) and 458 nm ($\varepsilon = 130\,M^{-1}\,cm^{-1}$), respectively, due to the spin-allowed $^1A_{1g} \rightarrow {}^1A_{2g}$ transition typical of square-planar d^8 species, which is consistent with the crystal structures observed by X-ray diffraction analysis. On the other hand, the absorption spectrum of **3a**, which is high-spin Ni^{II} complex in the solid state, shows a relatively weaker absorption band at 470 nm ($\varepsilon = 55\,M^{-1}\,cm^{-1}$) and very broad bands at 706 nm ($\varepsilon = 16\,M^{-1}\,cm^{-1}$) and 793 nm ($\varepsilon = 11\,M^{-1}\,cm^{-1}$) at 20 °C. These absorption features clearly demonstrate the coexistence of the two species in CH_3NO_2 solution, namely, high-spin octahedral configuration $[Ni^{II}(\mathbf{L^{O}})(CH_3CN)_2]^{2+}$ and low-spin square-planar configuration $[Ni^{II}(\mathbf{L^{O}})]^{2+}$ generated by dissociation of coordinating CH_3CN molecules in high-spin species. The fact that $[Ni^{II}(\mathbf{L^{O}})]^{2+}$ partially converted into $[Ni^{II}(\mathbf{L^{O}})(CH_3CN)_2]^{2+}$ in the presence of only two equivalents of CH_3CN molecules suggests the binding affinity of $[Ni^{II}(\mathbf{L^{O}})]^{2+}$ for external ligand is much higher than those of **1a** and **2a**, for which the absorption spectra remained unchanged upon addition of two equivalent of a stronger coordinating ligand such as pyridine.

Interconversion of the Spin State in Coordinating Solvents. The absorption spectra of **1a**–**3a** in coordinating solvents such as CH_3CN, DMF, and DMSO are different from those in noncoordinating solvent, CH_3NO_2 (Table 3). Ni^{II} complexes **1a** and **2a** show an intense band in the range of 460–490 nm together with lower energy broad bands exceeding 700 nm at room temperature. Such a phenomenon has been well known in tetradentate Ni^{II} complexes in coordinating solvents, including water,[6,8] where octahedral high-spin species $Ni^{II}L(X)_2$ and square-planar low-spin species $Ni^{II}L$ are coexisting as given by the following:

$$Ni^{II}L + 2X \rightleftarrows Ni^{II}L(X)_2 \quad (1)$$

It has been also reported that the equilibrium 1 is shifted to the right by increasing the coordinating tendency of X

Table 3. Absorption Data for Ni^{II} Complexes in Different Solvents at 20 °C

	λ_{max}/nm (ε/M^{-1} cm^{-1})		
Solvent	**1a**	**2a**	**3a**
CH_3NO_2	466 (167)	458 (130)	470 (55), 706 (16), 793 (11)
CH_3CN	468 (53), 723 (20)	483 (39), 807 (17)	516 (14), 738 (23)
	798 (12)	900sh (14)	792 (21)
DMF	521 (16), 731 (16)	538 (15), 810sh (17)	581 (11), 758 (20)
	749 (16), 915sh (7)	865 (19)	832 (22)
DMSO	460sh (70), 550sh (50)	460sh (50), 538 (43)	587 (25), 763 (33)
	760 (41), 805 (41), 925 (40)	815 (31), 880 (35)	800 (32), 862 (36)

Table 4. Equilibrium Constants (K) and Thermodynamic Data (ΔH^0/kJ mol^{-1} and ΔS^0/J K^{-1} mol^{-1}) for the Spin-State Interconversion of Ni^{II} Complexes **1a** and **2a**

	1a			**2a**		
Solvent	K	ΔH^0	ΔS^0	K	ΔH^0	ΔS^0
CH_3CN	0.27	−18.4	−48.9	0.14	−16.9	−37.7
DMF	28.0	−24.7	−56.4	28.2	−23.5	−53.2
DMSO	10.0	−26.6	−71.6	64.5	−24.7	−49.2

(X = solvent or anion) or by decreasing temperature.[6–8] In Figure 3 is shown the absorption spectra in an CH_3CN solution of **1a** observed at various temperatures as a typical example. Decreasing the temperature from 60 to −40 °C results in a decrease in the absorption intensity at 468 nm due to low-spin Ni^{II} species, with a concomitant increase of the bands at 723 and 798 nm due to high-spin species. The equilibrium constant for this reaction is given by eq 2, where A_L and A_H are the absorbance corresponding to the pure low-spin and high-spin Ni^{II} species, respectively.

$$K = [Ni^{II}\mathbf{L}^E(X)_2]/[Ni^{II}\mathbf{L}^E] = (A_L - A)/(A - A_H) \quad (2)$$
$$\mathbf{L}^E = \mathbf{L}^{NH} \text{ or } \mathbf{L}^S \text{ and } X = \text{solvent}$$

In all cases, however, A_L and A_H could not be determined directly since the reactions were unsaturated until the upper or lower limit of the temperature (due to the margin of equipment or melting/boiling point of the solvent). Alternatively, we adopted the absorbance observed in CH_3NO_2 of **1a** or **2a** as the corresponding A_L values, as reported by Fabbrizzi et al.[8] With regard to A_H, unfortunately, the values could not be estimated in these solvents. Therefore, A_H as well as the thermodynamic parameters ΔH^0 and ΔS^0 were determined by plotting the absorbance of the low-spin d–d band (≈470 nm) against $1/T$ and fitting these data with the following eq 3, which is derived from eqs 2 and 4 (Figure 3 inset).

$$A = \frac{A_L + A_H \cdot e^{-\frac{\Delta H^0}{RT} + \frac{\Delta S^0}{R}}}{1 + e^{-\frac{\Delta H^0}{RT} + \frac{\Delta S^0}{R}}} \quad (3)$$

$$\ln K = -\Delta H^0/RT + \Delta S^0/R \quad (4)$$

In Table 4 are listed K, ΔH^0, and ΔS^0 for the binding of each solvent to the low-spin square-planar Ni^{II} center. The binding strength of the solvent molecules toward Ni^{II} ion can be evaluated by the ΔH^0 term, which reflects the difference in the bonding energies between the metal center and the coordinating solvent at the axial positions. In other words, smaller $-\Delta H^0$ value means stronger in-plane interactions in the Ni^{II} complex. A comparison of $-\Delta H^0$ values between Ni^{II} complexes, $[Ni^{II}(\mathbf{L}^{NH})]^{2+}$ and $[Ni^{II}(\mathbf{L}^S)]^{2+}$, reveals that the latter has more stable in-plane character than the former. The order of the K values for $[Ni^{II}(\mathbf{L}^{NH})]^{2+}$ are not in agreement with those of ΔH^0 values, which may due to a compensating effect between ΔH^0 and ΔS^0. It should be noted that the linear dependences of $-\Delta H^0$ values toward Gutmann's Donor Number (DN),[29] which is a qualitative measure of Lewis basicity, were given in both cases of $[Ni^{II}(\mathbf{L}^{NH})]^{2+}$ and $[Ni^{II}(\mathbf{L}^S)]^{2+}$ as depicted in Figure 4, indicating the nature of σ interaction between the high-spin Ni^{II} center and the axial solvents.

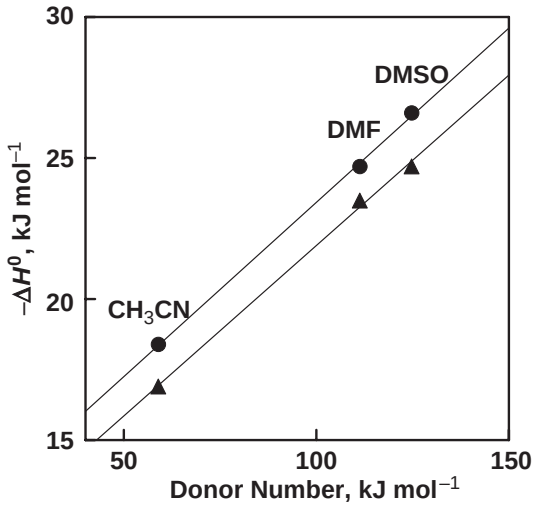

Figure 4. Plots of $-\Delta H_0$ for the spin-state interconversion in $[Ni^{II}(\mathbf{L}^{NH})](ClO_4)_2$ (**1a**, circle) and $[Ni^{II}(\mathbf{L}^S)](ClO_4)_2$ (**2a**, triangle) against Gutmann's Donor Number (DN) of the solvents.

Unlike the Ni^{II} complexes of $\mathbf{L}^{NH}$ and $\mathbf{L}^S$, high–low spin-state interconversion in Ni^{II} complexes of $\mathbf{L}^O$ was not recognized in any coordinating solvents described above even on increasing the temperature (e.g. up to 60 °C for CH_3CN). Thus, only the high-spin species exists in these solvents. Such a significantly higher binding constant of $[Ni^{II}(\mathbf{L}^O)]^{2+}$ with coordinating solvents causes an unusual redox behavior of **3a** as discussed below.

Redox Behaviors of Ni^{II} Complexes. The effect of heteroatom substitution in a series of macrocyclic ligands on redox behavior is of importance for the basic chemistry of Ni^{II} complexes. Cyclic voltammograms for **1a–3a** in Ar-saturated CH_3CN containing 0.1 M n-Bu_4NClO_4 are shown in Figure 5. The Ni^{II} complexes **1a** and **2a** exhibit a reversible reduction wave with peak separations of 80 and 100 mV, respectively, whereas, in the case of **3a**, the irreversible redox couple was observed with a significantly large peak separation of 460 mV. Although no EPR signal of the reduced products (electrochemically or chemically generated) were observed due to instability of the products on a time scale of minutes, the redox process of complexes **1a–3a** presented in Figure 5 is considered to be the metal center, Ni^{II}/Ni^{I}.[30] In addition, all complexes show irreversible oxidation waves, implying the thermodynamically unstable higher oxidation state of Ni^{III} with these macrocyclic ligands.

The potential of the Ni^{II}/Ni^{I} redox couple for the Ni^{II} complex with sulfur-containing ligand $\mathbf{L}^S$ ($E_{1/2} = -1.20$ V vs. $Ag/AgNO_3$) is more positive than that obtained for the Ni^{II} complex with N_4 donor ligand $\mathbf{L}^{NH}$ ($E_{1/2} = -1.48$ V vs. $Ag/AgNO_3$), that is a general trait in copper or nickel complexes having soft donor atom(s) such as S and P.[31] On the other hand, the redox behavior of **3a**, which forms a complete high-spin octahedral Ni^{II} complex in CH_3CN, shows an unusual voltammogram. A scan in the negative direction reveals a reduction wave at $E_{pc} = -1.76$ V vs. $Ag/AgNO_3$ due to reduction of the metal center. In this case, the nickel ion becomes Ni^{I}, that is a d^9, in which an electrostatic interaction

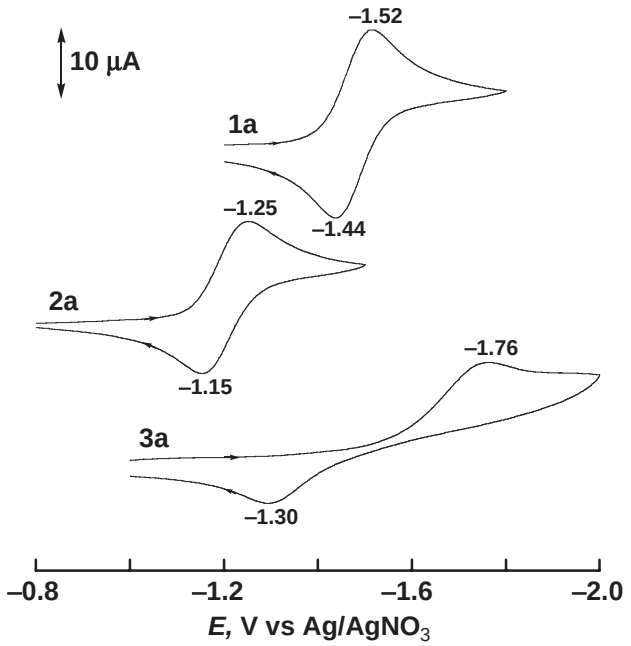

Figure 5. Cyclic voltammograms of $[Ni^{II}(\mathbf{L^{NH}})](ClO_4)_2$ (**1a**), $[Ni^{II}(\mathbf{L^{S}})](ClO_4)_2$ (**2a**), and $[Ni^{II}(\mathbf{L^{O}})(CH_3CN)_2](ClO_4)_2$ (**3a**) in deaerated CH_3CN containing 0.1 M n-Bu_4NClO_4 at room temperature; [Ni^{II} complex] = 5.0×10^{-3} M, working electrode Pt, counter electrode Pt wire, reference electrode Ag/0.01 M $AgNO_3$, scan rate 50 mV s^{-1}.

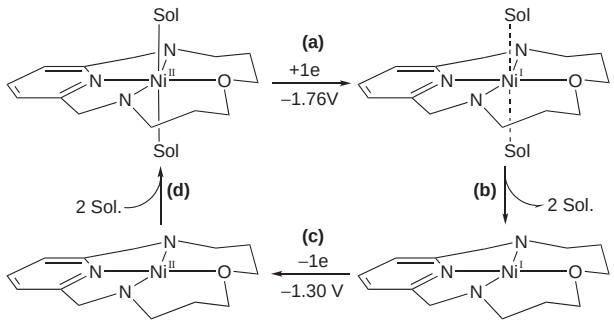

Scheme 2.

in the axial direction is destabilized (Jahn–Teller effect). The one-electron reduction of the high-spin Ni^{II} complex **3a**, thereby, results in the loss of its axial ligand (coordinating CH_3CN molecules) as depicted step (a) and (b) in Scheme 2. Then, the low-valent tetradentate Ni^{I} species thus formed is reoxidized to Ni^{II} at the potential of $E_{pa} = -1.30$ V vs. $Ag/AgNO_3$ (step (c)). The subsequent re-coordination of the solvent molecules to form the octahedral geometry (step (d)) was confirmed by a multisweep experiment, where a negligible change of the voltammogram was observed. Thus, from the irreversible redox behavior observed for **3a** it can be concluded that the dissociation and association of the axial ligands are accompanied by the reduction to Ni^{I} and the oxidation to Ni^{II}, respectively.[32]

Conclusion

Macrocyclic ligands containing a nitrogen or a sulfur atom at the 7-position, $\mathbf{L^{NH}}$ and $\mathbf{L^{S}}$, form low-spin square-planar Ni^{II} complexes $[Ni^{II}(\mathbf{L^{NH}})](ClO_4)_2$ (**1a**) and $[Ni^{II}(\mathbf{L^{S}})](ClO_4)_2$ (**2a**), whereas the oxygen-substituted analog $\mathbf{L^{O}}$ affords a high-spin octahedral Ni^{II} complex, $[Ni^{II}(\mathbf{L^{O}})(CH_3CN)_2](ClO_4)_2$ (**3a**), in solid state. In noncoordinating solvent, **1a** and **2a** are in a low-spin state, while the high-spin/low-spin interconversions of **1a** and **2a** are observed in coordinating solvents such as CH_3CN, DMF, and DMSO. The $-\Delta H^0$ value of the spin-interconversion from high to low species for **2a** smaller than that for **1a** indicates that the coordination of a sulfur atom enhances the in-plane character of the Ni^{II} center. In the case of **3a**, on the other hand, it exists only as a high-spin state with a wide range of temperature in coordinating solvents. This phenomenon may be due to weaker coordination of the ligand oxygen atom to the Ni^{II} center significantly increasing the Lewis acidity of the metal ion, which results in stabilization of axial coordination.[33] As a result, the cyclic voltammogram of **3a** shows a unique behavior, where the loss of its axial coordinating solvent occurs in the reduction of Ni^{II} to Ni^{I} and then the solvent again coordinates to the metal center upon re-oxidation. The result that the spin state and the redox behavior of the Ni^{II} complexes with a macrocyclic ligand can be controlled by the replacement of only one donor atom (NH, S, or O) will provide us valuable information for development of fluorescent indicators (e.g. for temperature, anions, and solvent polarity) or molecular switches.[34]

Experimental

2,6-Pyridinedicarbaldehyde and macrocyclic ligands $\mathbf{L^{NH}}$ and $\mathbf{L^{O}}$ were prepared according to published procedures.[21,22,26] Reagents and solvents used in this study were commercial products of the highest available purity and were further purified by standard methods, if necessary.[35] ^{1}H NMR and ^{13}C NMR spectra were recorded with a JEOL JNM-EX-270. J values are given in Hz. IR spectra were recorded with a SHIMADZU FTIR-8600PC. Mass spectra were obtained with a JEOL JMS-700. Magnetic susceptibility measurements were performed by using a quantum design SQUID in the temperature range of 2–300 K with an external applied field of 1000 G. Pascal's constants were used to determinate the constituent atom diamagnetism. Elemental analyses were conducted using a Yanaco CHN corder MT-5 or MT-6 (Because the Ni^{II} complexes used here, which contain one or two perchlorate anions, are explosive, the found values of the nitrogen atom are 1–8% off from the calculated values although the carbon and hydrogen values are within ±0.3%. Therefore, individual CHN data for these complexes are not described in this manuscript.). TLC analysis was carried out by using Silica gel 60 F_{254} (Merck). Column chloromatography was performed on silica gel (Wako Pure Chemical Industries, Ltd, Wakogel C-300) or alumina (Wako Pure Chemical Industries, Ltd, Alumina, Activated).

4-Thia-1,7-heptanediamine. A suspension of $NaBH_4$ (18.4 g, 0.49 mol) in THF (160 mL) was treated dropwise with a solution of CF_3COOH (55.3 g, 0.49 mol) in THF (40 mL) at room temperature. After stirring for 10 min, a solution of 4-thia-1,7-heptanedinitrile (8.0 g, 57 mmol) in THF (40 mL) was added to the mixture, and the resulting mixture was stirred at room temperature overnight. The mixture was acidified to pH <1 with 37% HCl_{aq} and filtrated to remove insoluble materials. The filtrate was then treated with 6 M NaOH until pH become 14 and extracted with EtOAc (3×80 mL). After concentration, the residue was dissolved in 37% HCl_{aq} (15 mL) and water was evaporated. The resulting white solid was washed with 2-propanol (50 mL × 3) and dissolved

again in 6 M NaOH (20 mL). The aqueous layer was extracted with EtOAc (80 mL × 3), and the combined extracts were dried over $MgSO_4$ and concentrated to give the diamine as a colorless oil (7.0 g, 88%). ^{1}H NMR (270 MHz, CD_3OD): δ 1.84 (m, 4H, CH_2), 2.61 (t, $J = 7.2$ Hz, 4H, CH_2), 2.88 (t, $J = 7.2$ Hz, 4H, CH_2); HRMS (EI^+) m/z 148.1038 (M^+), calcd for $C_6H_{16}N_2S_1$ 148.1034.

7-Thia-3,11,17-triazabicyclo[11.3.1]heptadeca-1(16),13(17),-14-triene (L^S). A solution of $Cu(NO_3)_2 \cdot 3H_2O$ (2.79 g, 11.53 mmol) in water (25 mL) was mixed with a solution of 2,6-pyridinedicarbaldehyde (1.56 g, 11.53 mmol) in ethanol (25 mL). A solution of 4-thia-1,7-heptanediamine (1.71 g, 11.53 mmol) in ethanol (20 mL) was added dropwise to the mixture. The resulting deep blue solution was refluxed for 3 h. After cooling to 5 °C, $NaBH_4$ (1.74 g, 46.1 mmol) was added in small portions. The mixture was stirred at room temperature for 30 min, and at 50 °C for 30 min, and then was allowed to stand at room temperature overnight. Copper(II) was removed by treating the reaction mixture with $Na_2S \cdot 9H_2O$ (3.16 g, 13.2 mmol) followed by heating at 50 °C for 30 min. After cooling, copper(II) sulfide was removed by filtration through a pad of Celite. The filtrate was extracted with dichloromethane (3 × 50 mL), and the combined extracts were dried with $MgSO_4$ and concentrated in vacuo. The residue was purified by SiO_2 column chromatography (EtOAc:MeOH 1:1 containing 1% triethylamine) to give the desired product $\mathbf{L^S}$ (908 mg, 31%) as a white powder. δ_H (270 MHz, $CDCl_3$): 1.82 (m, 4H, CH_2), 2.58 (t, $J = 5.4$ Hz, 4H, CH_2), 3.55 (t, $J = 5.6$ Hz, 4H, CH_2), 3.89 (s, 4H, CH_2), 7.00 (d, $J = 7.6$ Hz, 2H, $CH_{aromatic}$), 7.52 (t, $J = 7.6$ Hz, 1H, $CH_{aromatic}$); δ_C (68 MHz, $CDCl_3$): 29.73, 45.27, 54.30, 68.21, 120.63, 136.40, 159.05; HRMS (EI^+) m/z 251.1450 (M^+), calcd for $C_{13}H_{21}N_3S_1$ 251.1456.

$[Ni^{II}(L^{NH})](ClO_4)_2$ (1a). A solution of $Ni(ClO_4)_2 \cdot 6H_2O$ (460 mg, 1.26 mmol) in methanol (5 mL) was added to a solution of ligand $\mathbf{L^{NH}}$ (316 mg, 1.26 mmol) in methanol (10 mL), and the mixture was thoroughly stirred at room temperature, during which a brown powder precipitated. The powder was collected by suction and washed with cold methanol. Recrystallization of the crude product by vapor diffusion of diethyl ether into an CH_3CN solution of the complex gave red-brown crystals of **1a** (284 mg, 76%). FT-IR (KBr): 1093 (ClO_4^-) cm^{-1}; FAB-MS (glycerol): m/z 391 $[M - ClO_4^-]^+$.

$[Ni^{II}(L^S)](ClO_4)_2$ (2a). This compound was prepared in a similar manner to that described for **1a** using $\mathbf{L^S}$ (85 mg, 0.34 mmol) and $Ni(ClO_4)_2 \cdot 6H_2O$ (124 mg, 0.34 mmol). Yield 99 mg (58%), red-brown crystals. FT-IR (KBr): 1089 (ClO_4^-) cm^{-1}; FAB-MS (glycerol): m/z 309 $[M - 2ClO_4^-]^+$.

$[Ni^{II}(L^S)](ClO_4)(BPh_4)$ (2b). To a warm solution of **2a** (40 mg, 79 μmol) in methanol (3 mL) was added $NaBPh_4$ (100 mg, 292 μmol) with stirring. A brown powder thus precipitated was collected and recrystallized by vapor diffusion of diethyl ether into an CH_3CN solution of the complex to give red-brown crystals. Yield 51 mg (88%), red-brown crystals. FT-IR (KBr): 1061 (ClO_4^-), 738, 711 cm^{-1} (BPh_4^-); FAB-MS (glycerol): m/z 309 $[M - ClO_4^- - BPh_4^-]^+$.

$[Ni^{II}(L^O)(CH_3CN)_2](ClO_4)_2$ (3a). This compound was prepared in a similar manner to that described for **1a** using $\mathbf{L^O}$ (178 mg, 0.71 mmol) and $Ni(ClO_4)_2 \cdot 6H_2O$ (260 mg, 0.71 mmol). Yield 284 mg (76%), pale purple crystals. FT-IR (KBr): 1108 (ClO_4) cm^{-1}; FAB-MS (NBA): m/z 392 $[M - ClO_4^-]^+$.

$[Ni^{II}(L^O)(CH_3CN)_2](ClO_4)(BPh_4)$ (3b). The counter anion of **3a** (40 mg, 81 μmol) was exchanged with $NaBPh_4$ (111 mg, 325 μmol) according to the same procedure described for the synthesis of **2b**. Yield 55 mg (85%), pale purple crystals. FT-IR (KBr): 1103 (ClO_4^-), 733, 711 cm^{-1} (BPh_4^-); FAB-MS (NBA): m/z 293 $[M - ClO_4^- - BPh_4^-]^+$.

Caution: These perchlorate complexes are explosive. In fact, explosions have been found in the elemental analysis of the nickel complexes containing perchlorate ions. The use of small amount of materials is strongly recommended.

X-ray Structure Determination. The single crystals were sealed in glass capillary tubes containing the mother liquid. Data of X-ray diffraction for $[Ni^{II}(\mathbf{L^{NH}})](ClO_4)_2$ (**1a**), $[Ni^{II}(\mathbf{L^S})](ClO_4)(BPh_4)$ (**2b**), and $[Ni^{II}(\mathbf{L^O})(CH_3CN)_2](ClO_4)(BPh_4)$ (**3b**) were collected by using a Rigaku RAXIS-RAPID imaging plate area detector with graphite monochromated Mo Kα radiation ($\lambda = 0.71075$ Å) to $2\theta_{max}$ of 54.9° for **1a** and 55.0° for **2b** and **3b**. All data were corrected for Lorentz and polarization effects. All the crystallographic calculations were performed by using a crystal structure software package of the Rigaku Corporation and Molecular Structure Corporation [Crystal Structure: *Crystal Structure Analysis Package version 3.8.1*, Rigaku Corp. and Molecular Structure Corp., **2005**]. The crystal structure was solved by direct methods and refined by full-matrix least squares using SIR-97.[36] All non-hydrogen atoms were refined anisotropically. Hydrogen atoms were fixed at calculated positions and refined using the riding model. Crystallographic data have been deposited with Cambridge Crystallographic Data Centre: Deposition numbers CCDC 650352–650354 for compounds **1a**, **2b**, and **3b**, respectively. Copies of the data can be obtained free of charge via http://www.ccdc.cam.ac.uk/conts/retrieving.html (or from the Cambridge Crystallographic Data Centre, 12, Union Road, Cambridge, CB2 1EZ, UK; Fax: +44 1223 336033; e-mail: deposit@ccdc.cam.ac.uk).

Electronic Spectroscopy. The UV–vis absorption spectra of the nickel(II) complexes were recorded on a Hewlett-Packard 8453 spectrometer with a UV cell (1 cm path length, sealed tightly with a silicon rubber cap), which was held in a Unisoku thermostatic cell holder designed for high-to-low temperature measurements. The cell was kept at the desired temperature for several minutes prior to measurement.

Cyclic Voltammetry (CV). Cyclic voltammetric measurements were performed on an ALS-600B electrochemical analyzer in deaerated CH_3CN containing 0.1 M n-Bu_4NClO_4 as a supporting electrolyte. A Pt working electrode (BAS Inc.) was polished with 0.05 μm polishing alumina (BAS Inc.) and rinsed with acetone before use. The counter electrode was a platinum wire. The measured potentials were recorded with respect to a $Ag/AgNO_3$ (0.01 M) reference electrode. All electrochemical measurements were carried out under Ar atmosphere.

This work was financially supported by Grant-in-Aid for Young Scientists (B) (No. 17750155) from the Ministry of Education, Culture, Sports, Science and Technology, Japan.

References

1 M. A. Halcrow, G. Christou, *Chem. Rev.* **1994**, *94*, 2421.
2 I. Zilbermann, E. Maimon, H. Cohen, D. Meyerstein, *Chem. Rev.* **2005**, *105*, 2609.
3 H. Elias, *Coord. Chem. Rev.* **1999**, *187*, 37.
4 a) L. Fabbrizzi, F. Foti, M. Licchelli, A. Poggi, A. Taglietti, M. Vázquez, *Adv. Inorg. Chem.* **2006**, *59*, 81. b) V. Amendola, L. Fabbrizzi, M. Licchelli, C. Mangano, P. Pallavicini, L. Parodi, A. Poggi, *Coord. Chem. Rev.* **1999**, *190–192*, 649. c) V. Amendola, L. Fabbrizzi, F. Foti, M. Licchelli, C. Mangano, P.

Pallavicini, A. Poggi, D. Sacchi, A. Taglietti, *Coord. Chem. Rev.* **2006**, *250*, 273. d) L. Fabbrizzi, M. Licchelli, P. Pallavicini, L. Parodi, *Angew. Chem., Int. Ed.* **1998**, *37*, 800. e) M. Engeser, L. Fabbrizzi, M. Licchelli, D. Sacchi, *Chem. Commun.* **1999**, 1191.

5 C. K. Jørgensen, *Acta Chem. Scand.* **1957**, *11*, 399.

6 L. Sabatini, L. Fabbrizzi, *Inorg. Chem.* **1979**, *18*, 438.

7 B. Bosnich, M. L. Tobe, G. A. Webb, *Inorg. Chem.* **1965**, *4*, 1109.

8 M. Boiocchi, L. Fabbrizzi, F. Foti, M. Vazquez, *Dalton Trans.* **2004**, 2616.

9 J. D. Vitiello, E. J. Billo, *Inorg. Chem.* **1980**, *19*, 3477.

10 U. Ermler, W. Grabarse, S. Shima, M. Goubeaud, R. K. Thauer, *Science* **1997**, *278*, 1457.

11 C. L. Hamilton, R. A. Scott, M. K. Johnson, *J. Biol. Chem.* **1989**, *264*, 11605.

12 A. K. Shiemke, J. A. Shelnutt, R. A. Scott, *J. Biol. Chem.* **1989**, *264*, 11236.

13 C. Holliger, A. J. Pierik, E. J. Reijerse, W. R. Hagen, *J. Am. Chem. Soc.* **1993**, *115*, 5651.

14 J. Telser, Y. C. Fann, M. W. Renner, J. Fajer, S. Wang, H. Zhang, R. A. Scott, B. M. Hoffman, *J. Am. Chem. Soc.* **1997**, *119*, 733.

15 M. P. Suh, *Adv. Inorg. Chem.* **1997**, *44*, 93.

16 K. Kobiro, A. Nakayama, T. Hiro, M. Suwa, Y. Tobe, *Inorg. Chem.* **1992**, *31*, 676.

17 C. P. Kulatilleke, S. N. Goldie, M. J. Heeg, L. A. Ochrymowycz, D. B. Rorabacher, *Inorg. Chem.* **2000**, *39*, 1444.

18 M. A. Donnelly, M. Zimmer, *Inorg. Chem.* **1999**, *38*, 1650.

19 a) V. Félix, M. J. Calhorda, J. Costa, R. Delgado, C. Brito, M. T. Duarte, T. Arcos, M. G. B. Drew, *J. Chem. Soc., Dalton Trans.* **1996**, 4543. b) V. Félix, J. Costa, R. Delgado, M. G. B. Drew, M. T. Duarte, C. Resende, *J. Chem. Soc., Dalton Trans.* **2001**, 1462.

20 a) A. Tamayo, J. Casabo, L. Escriche, C. Lodeiro, B. Covelo, C. D. Brondino, R. Kivekas, R. Sillampaa, *Inorg. Chem.* **2006**, *45*, 1140. b) A. Tamayo, L. Escriche, C. Lodeiro, J. Ribas-Arino, J. Ribas, B. Covelo, J. Casabo, *Inorg. Chem.* **2006**, *45*, 7621.

21 J. Costa, R. Delgado, *Inorg. Chem.* **1993**, *32*, 5257.

22 K. P. Balakrishnan, H. A. A. Omar, P. Moore, N. W. Alcock, G. A. Pike, *J. Chem. Soc., Dalton Trans.* **1990**, 2965.

23 M. Vetrichelvan, Y. H. Lai, K. F. Mok, *Eur. J. Inorg. Chem.* **2004**, 2086.

24 A. M. Herrera, R. J. Staples, S. V. Kryatov, A. Y. Nazarenko, E. V. Rybak-Akimova, *Dalton Trans.* **2003**, 846.

25 G. R. Newkome, J. D. Sauer, J. M. Roper, D. C. Hager, *Chem. Rev.* **1977**, *77*, 513.

26 S. Autzen, H. G. Korth, R. Boese, H. de Groot, R. Sustmann, *Eur. J. Inorg. Chem.* **2003**, 1401.

27 G. Musie, J. H. Reibenspies, M. Y. Darensbourg, *Inorg. Chem.* **1998**, *37*, 302.

28 V. E. Kaasjager, L. Puglisi, E. Bouwman, W. L. Driessen, J. Reedijk, *Inorg. Chim. Acta* **2000**, *310*, 183.

29 V. Gutmann, *Coord. Chem. Rev.* **1976**, *18*, 225.

30 F. V. Lovecchio, E. S. Gore, D. H. Busch, *J. Am. Chem. Soc.* **1974**, *96*, 3109.

31 T. L. James, D. M. Smith, R. H. Holm, *Inorg. Chem.* **1994**, *33*, 4869.

32 Similar redox behavior have been reported in mono- or dinuclear cobalt(III) schiff base complexes, in which the axial coordinating ligands are lost when Co^{III} ions are reduced: A. Bottcher, T. Takeuchi, K. I. Hardcastle, T. J. Meade, H. B. Gray, D. Cwikel, M. Kapon, Z. Dori, *Inorg. Chem.* **1997**, *36*, 2498; H. Shimakoshi, T. Takemoto, I. Aritome, Y. Hisaeda, *Inorg. Chem.* **2005**, *44*, 9134.

33 H. Ohtsu, K. Tanaka, *Inorg. Chem.* **2004**, *43*, 3024.

34 O. Kahn, J. Krober, C. Jay, *Adv. Mater.* **1992**, *4*, 718.

35 W. L. F. Armarego, C. L. L. Chai, *Purification of Laboratory Chemicals*, 5th ed., Butterworth-Heinemann, Boston, **2003**.

36 SIR-97: A. Altomare, M. C. Burla, M. Camalli, G. L. Cascarano, C. Giacovazzo, A. Guagliardi, A. G. G. Moliterni, G. Polidori, R. Spagna, *J. Appl. Crystallogr.* **1999**, *32*, 115.